

Supplemental Material for

Ji, X., J. D. Neelin and C. R. Mechoso, 2015: El Niño/Southern Oscillation Sea Level Pressure Anomalies in the Western Pacific: Why are they there? *J. Climate*.

Here we examine the robustness of essential features presented in the main text with a number of alternate or extended diagnostics. Figure S1 shows anomalies in SLP and its baroclinic and barotropic components, as well as the tropospheric temperature, similar to Figs. 1 and 2 of the main text, but computed by regressing the monthly mean fields onto Niño 3.4 through the full annual cycle for the 27-year (1982-2008) period from the NCEP-NCAR reanalysis. Similar patterns are obtained, albeit with weaker magnitudes in this annual case as for the DJF case in the main text. This suggests that the spatial discrepancy between regions of larger SLP anomalies and tropospheric temperature anomalies associated with ENSO in the tropical Pacific is robust throughout the year, despite the seasonal asymmetries of the subtropical circulation and associated baroclinic and barotropic interactions in the subtropics.

Figure S2 shows the calculations of SLP, SLP baroclinic component, and SLP barotropic component with equation (4) in the main text using NCEP-NCAR reanalysis geopotential height. Compared with Fig. S1 panels (d) (e) and (f), using equation (5) of the main text, respectively, the two methods for decomposition of SLP anomalies are in good agreement for all major features.

It is also useful to have an estimate of how the teleconnection pattern translates into surface wind. Figures S3a and S4a show the regression of NCEP-NCAR reanalysis surface zonal wind and vector surface wind onto Niño3.4, respectively (through the full annual cycle, as in Fig. S1). Figures S3b and S4b show the reconstructed winds from the NCEP 1000hPa geopotential field using simple damping assumptions (Stevens et al. 2002). The reconstruction compares to the actual surface winds sufficiently well over oceans to motivate reconstructing separately the baroclinic and barotropic components from the respective geopotential contributions. In Figures S3c, d, the baroclinic zonal wind contribution near the equator in the tropical Pacific is substantially larger than the barotropic contribution, so an approximation that would include only the baroclinic mode would have qualitatively useful features. However, the barotropic contribution is not negligible even in the deep tropics. Furthermore, in the subtropics, the barotropic contribution considerably cancels the baroclinic contribution to the surface wind, as one would expect when surface drag is effective at damping the near surface baroclinic wind component and spinning up a barotropic wind component.

In Figure S5, we further decompose the *baroclinic* component of SLP (Fig. S1e) into its free troposphere (900-150hPa) contribution (Fig. S5b) and boundary layer (1000-900hPa) contribution (Fig. S5d). The corresponding decomposition of the tropospheric temperature anomalies in Fig. S1c, i.e., the vertical average over free troposphere and boundary layer, respectively, is also shown in Figs. S5a and S5c. The tropospheric temperature anomalies in the free troposphere and the boundary layer have similar magnitudes but very different patterns, with the latter resembling the SST anomalies in

Fig. S1a. However, the baroclinic contribution to SLP anomalies from the free tropospheric temperature is much larger than that of the boundary layer due to the greater depth of the free troposphere. Notice that in either case, the contributions to SLP anomalies in the western Pacific are very weak.

Figure S6 shows the winter season (December, January and February) mean tropospheric temperature anomalies, SLP anomalies and the baroclinic and barotropic SLP anomalies associated with ENSO using the example of the GFDL HiRAM-C360 model. Overall, the results obtained with the GFDL HiRAM-C360 (Fig. S6) are similar to those from the NCEP-NCAR reanalysis (Figs. 1 and 2 of the main text) in large-scale patterns and magnitudes. In particular, the positive SLP anomalies in the western Pacific are due to the barotropic contribution since the baroclinic contribution has the opposite sign and is small. Details of the spatial pattern within the western Pacific differ slightly, but overall the barotropic contribution is substantial and spreads widely through the tropical band in the model simulation as in reanalysis.

References:

Stevens, B., J. J. Duan, J. C. McWilliams, M. Munnich, and J. D. Neelin, 2002: Entrainment, Rayleigh friction, and boundary layer winds over the tropical Pacific. *J. Climate*, **15**, 30–44, doi:10.1175/1520-0442(2002)015,0030:ERFABL.2.0.CO;2.

Supplemental Figures:

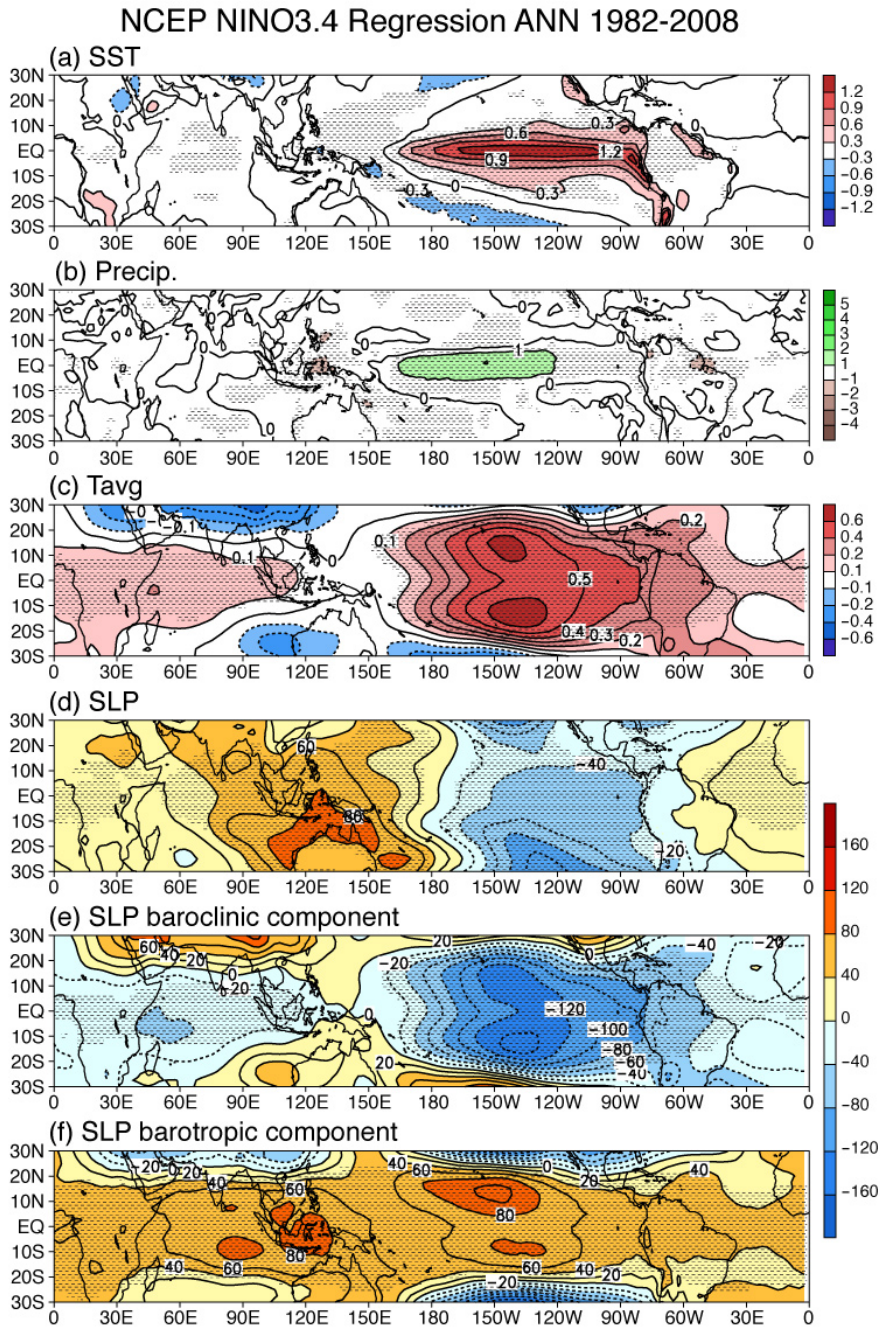


Fig. S1 (a) SST ($K \text{ } ^\circ\text{C}^{-1}$), (b) precipitation ($\text{mm day}^{-1} \text{ } ^\circ\text{C}^{-1}$), (c) tropospheric temperature ($K \text{ } ^\circ\text{C}^{-1}$), (d) SLP ($\text{Pa } ^\circ\text{C}^{-1}$), (e) SLP baroclinic component ($\text{Pa } ^\circ\text{C}^{-1}$), and (f) SLP barotropic component ($\text{Pa } ^\circ\text{C}^{-1}$) from NCEP-NCAR reanalysis regression of monthly anomalies onto Niño3.4 over the full annual cycle (referred to as the *annual case*), with a two-tailed t test applied to the regression values and stippled at 99% confidence.

NCEP NINO3.4 Regression ANN 1982-2008

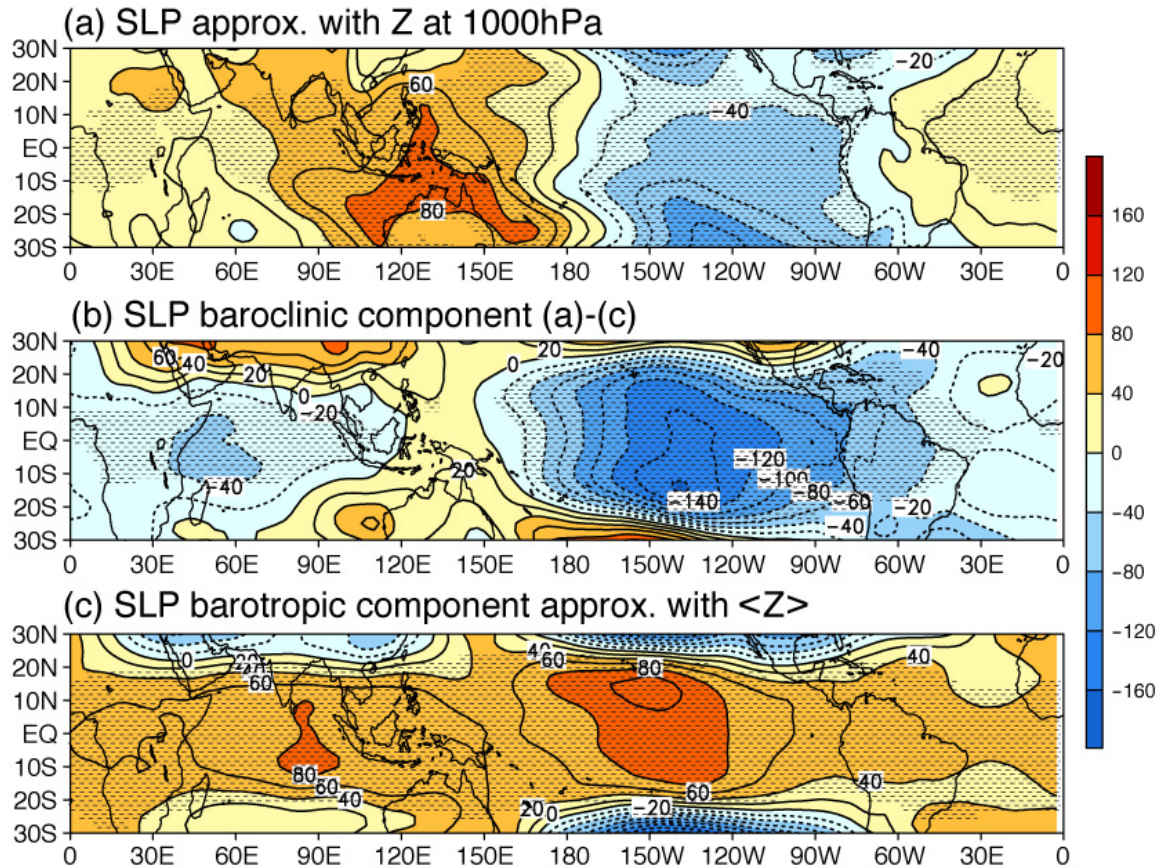


Fig. S2 (a) SLP ($\text{Pa } ^\circ\text{C}^{-1}$), (b) SLP baroclinic component ($\text{Pa } ^\circ\text{C}^{-1}$), and (c) SLP barotropic component ($\text{Pa } ^\circ\text{C}^{-1}$), calculated with equation (4) of the main text, from NCEP-NCAR reanalysis geopotential height (Z) *annual case* regression onto Niño3.4, with a two-tailed t test applied to the regression values and stippled at 99% confidence.

NCEP NINO3.4 Regression ANN 1982-2008

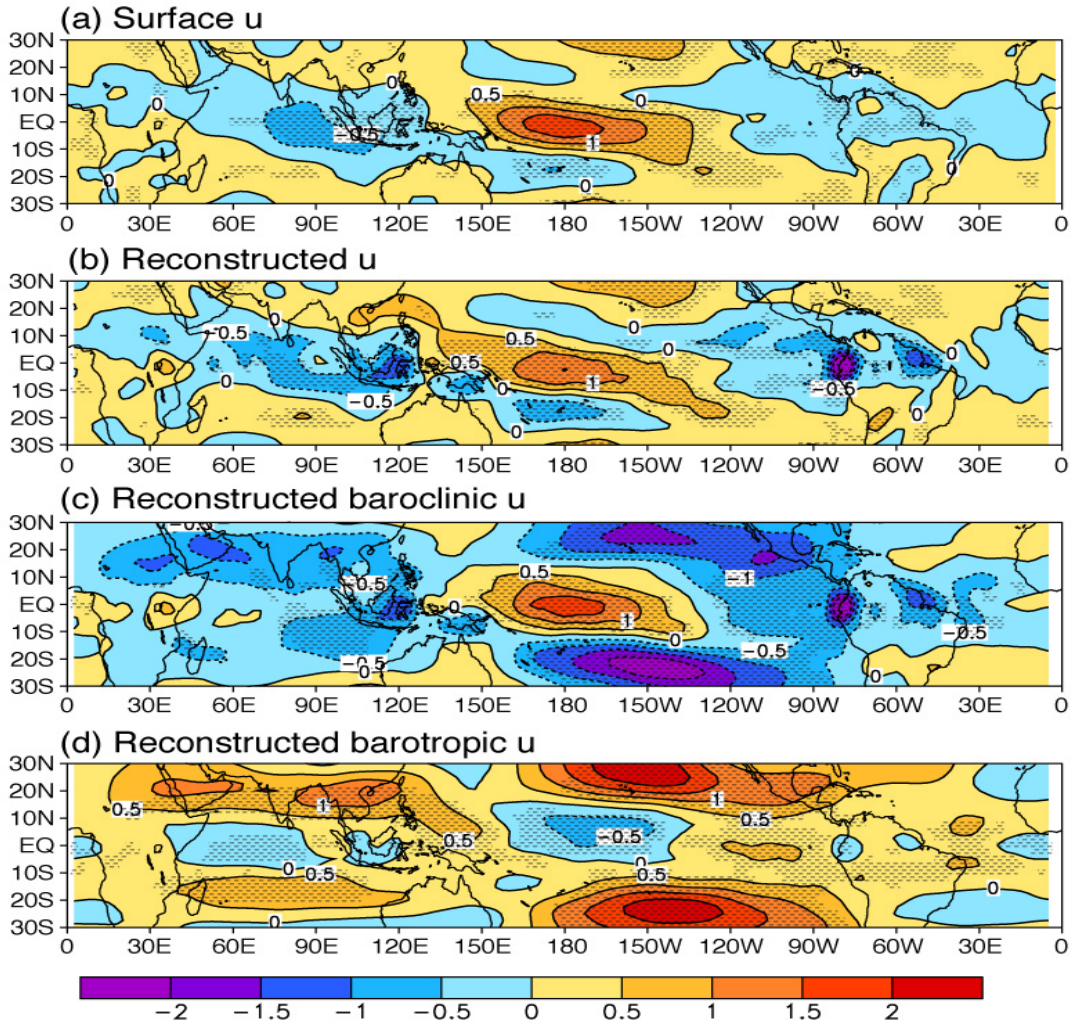


Fig. S3 (a) Zonal wind, (b) zonal wind reconstructed from geopotential height at 1000hPa, (c) zonal wind baroclinic component reconstructed from baroclinic geopotential height at 1000hPa, (d) zonal wind barotropic component reconstructed from barotropic geopotential height at 1000hPa from NCEP-NCAR reanalysis *annual case* regression onto Niño3.4, with a two-tailed t test applied to the regression values and stippled at 99% confidence. The reconstructed wind is a solution to the equations $-\epsilon u + fv = -\partial_x \phi$ and $-\epsilon v - fu = -\partial_y \phi$, forced by the specified 1000hPa geopotential, where an assumed bulk damping due to surface stress is used, with a value $\epsilon = (1\text{day})^{-1}$. The units are m s^{-1} .

NCEP NINO3.4 Regression ANN 1982-2008

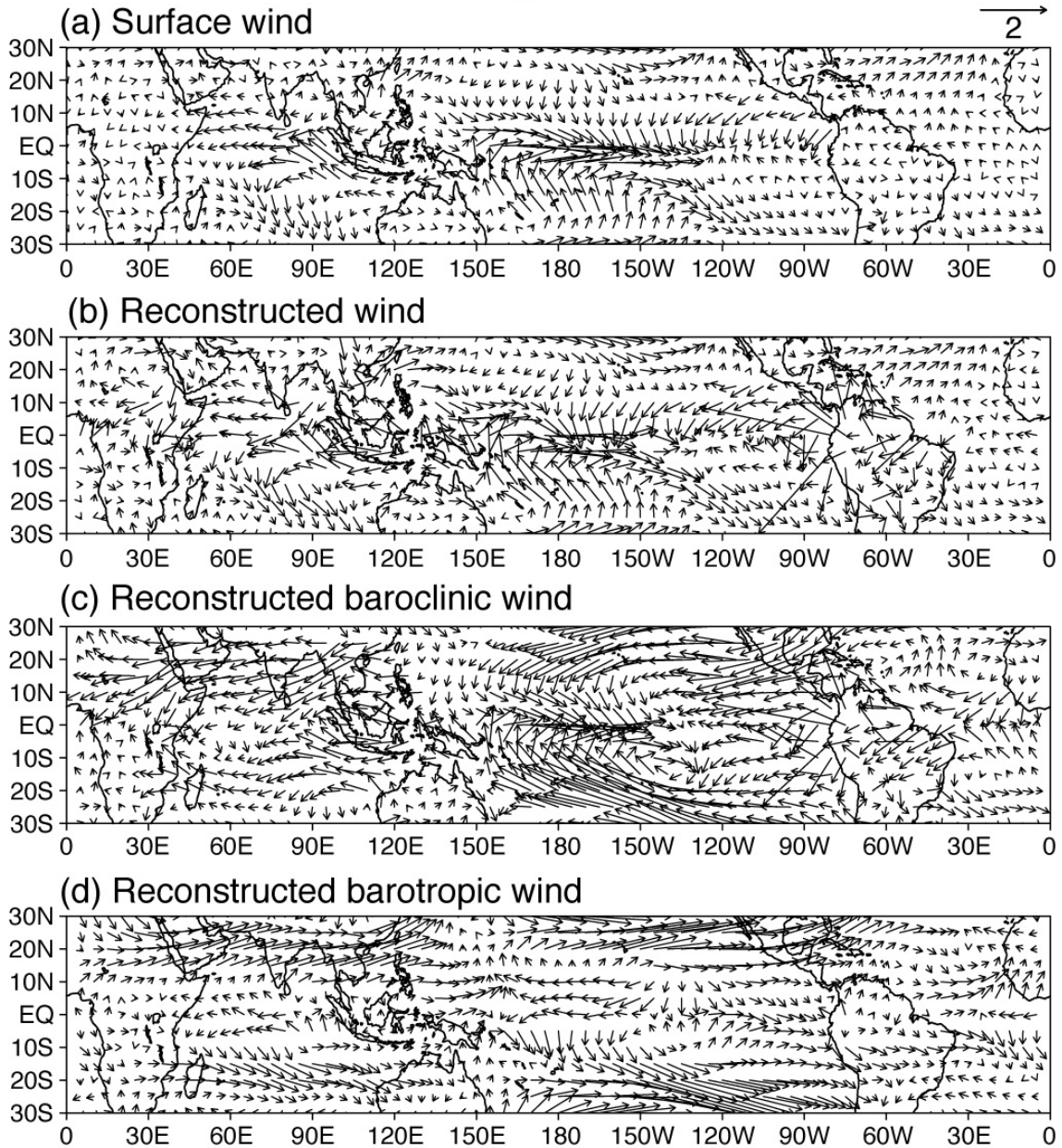


Fig. S4 (a) Surface wind, (b) surface wind reconstructed from geopotential height at 1000hPa, (c) surface wind baroclinic component reconstructed from baroclinic geopotential height at 1000hPa, (d) surface wind barotropic component reconstructed from barotropic geopotential height at 1000hPa from NCEP-NCAR reanalysis *annual case* regression onto Niño3.4. The units are m s^{-1} .

NCEP NINO3.4 Regression ANN 1982-2008

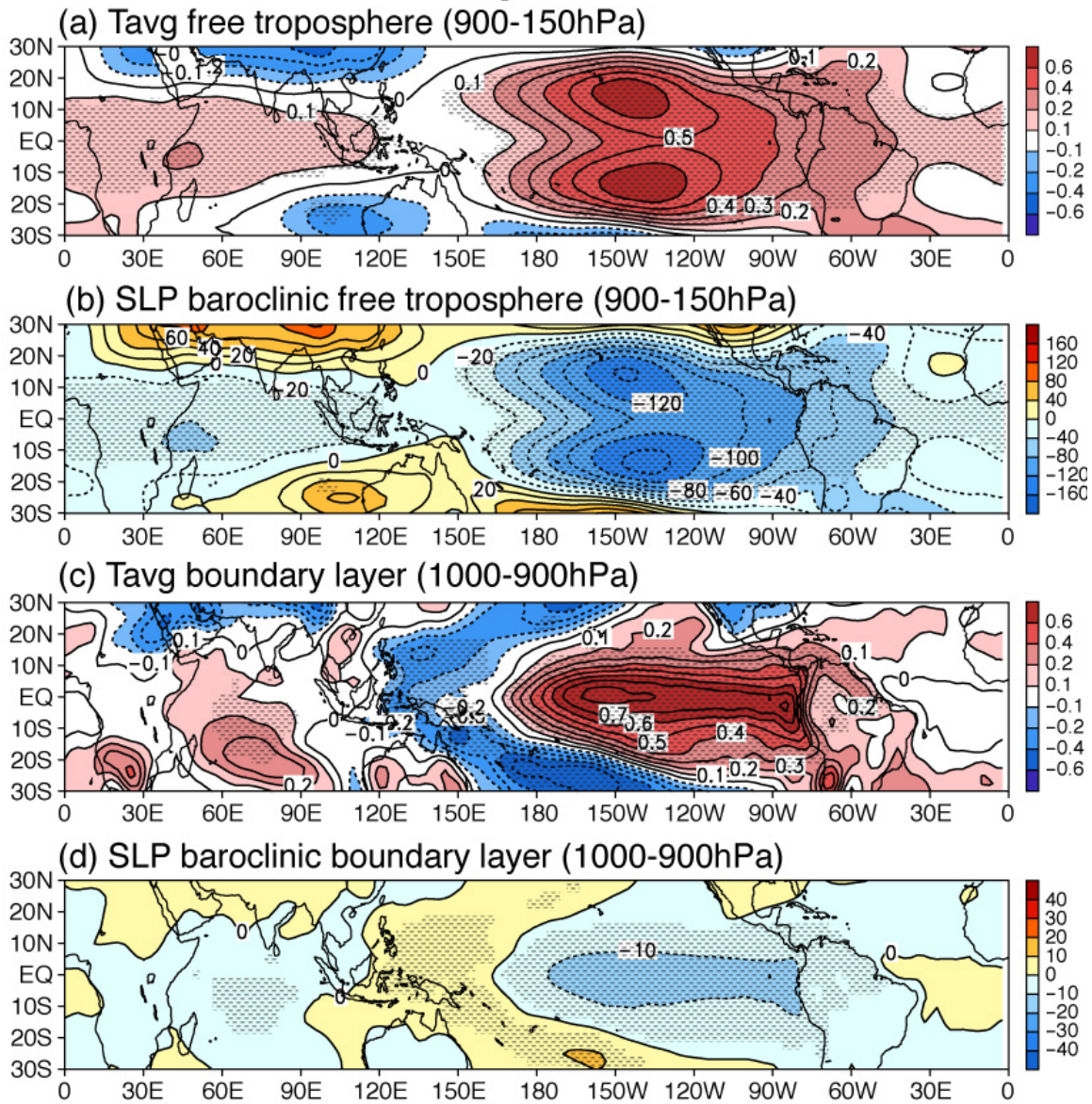


Fig. S5 (a) Tropospheric temperature average over free troposphere (900-150hPa) ($\text{K } ^\circ\text{C}^{-1}$), (b) SLP baroclinic free troposphere (900-150hPa) component ($\text{Pa } ^\circ\text{C}^{-1}$), (c) tropospheric temperature average over boundary layer (1000-900hPa) ($\text{K } ^\circ\text{C}^{-1}$) and (d) SLP baroclinic boundary layer (1000-900hPa) component ($\text{Pa } ^\circ\text{C}^{-1}$), from NCEP-NCAR reanalysis *annual case* regression onto Niño3.4, with a two-tailed t test applied to the regression values and stippled at 99% confidence.

GFDL-HIRAM-C360 NINO3.4 Regression DJF 1982-2008

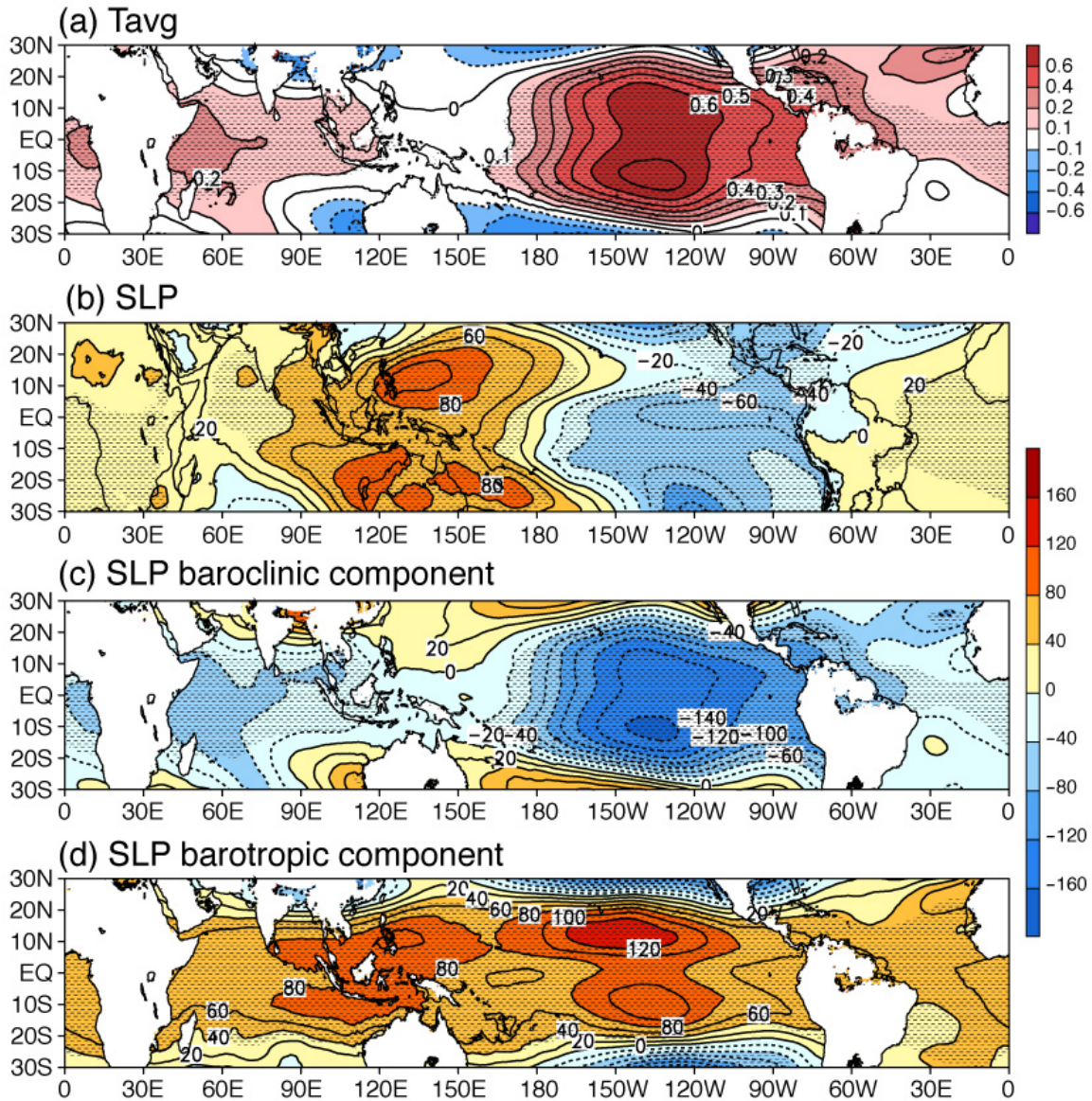


Fig. S6 (a) Tropospheric temperature ($K \text{ } ^\circ\text{C}^{-1}$), (b) SLP ($\text{Pa } ^\circ\text{C}^{-1}$), (c) SLP baroclinic component ($\text{Pa } ^\circ\text{C}^{-1}$), and (d) SLP barotropic component ($\text{Pa } ^\circ\text{C}^{-1}$) from GFDL HiRAM-C360 run with prescribed SSTs DJF regression onto Niño3.4, with a two-tailed t test applied to the regression values and stippled at 99% confidence. Note in (a), (c), and (d), land points for which temperature does not extend to 1000hPa are masked; SLP interpolation in (b) is as provided by the modeling center.